

# N-cadherin upregulation mediates adaptive radioresistance in glioblastoma

Satoru Osuka,<sup>1,2</sup> Dan Zhu<sup>2</sup>, Zhaobin Zhang,<sup>2</sup> Chaoxi Li,<sup>1</sup> Christian T. Stackhouse,<sup>1,3</sup> Oltea Sampetean,<sup>4</sup> Jeffrey J. Olson,<sup>2</sup> G. Yancey Gillespie,<sup>1</sup> Hideyuki Saya,<sup>4</sup> Christopher D. Willey,<sup>3</sup> and Erwin G. Van Meir<sup>1,2</sup>

<sup>1</sup>Department of Neurosurgery, School of Medicine and O'Neal Comprehensive Cancer Center, University of Alabama at Birmingham, Birmingham, Alabama, USA. <sup>2</sup>Laboratory of Molecular Neuro-Oncology, Department of Neurosurgery, School of Medicine and Winship Cancer Institute, Emory University, Atlanta, Georgia, USA. <sup>3</sup>Department of Radiation Oncology, University of Alabama at Birmingham, Birmingham, USA. <sup>4</sup>Division of Gene Regulation, Institute for Advanced Medical Research, Keio University School of Medicine, Tokyo, Japan.

**Glioblastoma (GBM) is composed of heterogeneous tumor cell populations, including those with stem cell properties, termed glioma stem cells (GSCs). GSCs are innately less radiation sensitive than the tumor bulk and are believed to drive GBM formation and recurrence after repeated irradiation. However, it is unclear how GSCs adapt to escape the toxicity of repeated irradiation used in clinical practice. To identify important mediators of adaptive radioresistance in GBM, we generated radioresistant human and mouse GSCs by exposing them to repeat cycles of irradiation. Surviving subpopulations acquired strong radioresistance in vivo, which was accompanied by a reduction in cell proliferation and an increase in cell-cell adhesion and N-cadherin expression. Increasing N-cadherin expression rendered parental GSCs radioresistant, reduced their proliferation, and increased their stemness and intercellular adhesive properties. Conversely, radioresistant GSCs lost their acquired phenotypes upon CRISPR/Cas9-mediated knockout of N-cadherin. Mechanistically, elevated N-cadherin expression resulted in the accumulation of  $\beta$ -catenin at the cell surface, which suppressed Wnt/ $\beta$ -catenin proliferative signaling, reduced neural differentiation, and protected against apoptosis through Clusterin secretion. N-cadherin upregulation was induced by radiation-induced IGF1 secretion, and the radiation resistance phenotype could be reverted with picropodophyllin, a clinically applicable blood-brain-barrier permeable IGF1 receptor inhibitor, supporting clinical translation.**

## Introduction

Glioblastoma (GBM) is an important health problem and major clinical challenge. GBM is the most aggressive brain tumor in adults, with a median overall survival of less than 2 years. Poor prognosis of patients with GBM is due to tumor cells that survive after repeated irradiation included in standard therapeutic regimens (5 days/week at 1–2 Gy/day, total 60 Gy). Prior studies have revealed that radioresistant glioma cells are endowed with characteristics of stem cells, including relative slow growth and high self-renewal capacity (1–3). Currently, there are no effective therapies to target radioresistant glioma stem cells (GSCs). Therefore, deciphering the molecular pathways that underlie resistance is critical to developing new effective therapies for GSCs.

Mitotic plasticity is an important mechanism of adaptive therapeutic resistance in cancer. The effectiveness of radiation therapy is dependent on the proliferation rate of irradiated cells (4, 5). This effect provides the rationale for selective targeting of fast-growing cancer cells over quiescent normal tissue. However, a small fraction of cancer cells can acquire a state of reduced proliferation during repeated chemoradiotherapy (6, 7). Slower proliferation is an important property for the maintenance of neural

stem cells (NSCs) (8, 9). As NSCs can serve as cells of origin for GSC generation, the latter may coopt the dormancy pathways of NSCs to achieve therapeutic resistance (1–3, 10). Recent single-cell RNA-seq analysis of human GBM samples has shown that tumor cells with an elevated stem cell phenotype display slower proliferation compared with neighboring cells (11). However, the molecular mechanisms through which GSCs establish a state of slow growth and maintain their stemness are poorly understood.

Cell-cell adhesion is a biological property that supports tumor formation, and can participate in the induction of therapeutic resistance (12). Recently, cell-cell and cell-matrix adhesion have become recognized as necessary mechanical properties associated with the maintenance of the stemness properties of several types of stem cells, including NSCs and cancer stem cells (13–15). Cell-cell contact is especially important to keep NSCs close to their niche, where they can receive instructive signals (16). The epithelial to mesenchymal transition (EMT) is an important biological process that reprograms cell adhesion properties. Interestingly, recent studies have shown that GSCs with a mesenchymal phenotype display increased therapeutic resistance (17, 18). However, the role of EMT-like signaling in therapeutic resistance of GBM is unknown.

N-cadherin (N-cad) is a transmembrane adhesion protein and marker of the EMT. It also functions as an important cell-cell adhesion molecule in the brain (19, 20). Both glioma cells and GSCs express N-cad (21–23), and N-cad has a role in brain tumor invasion (23, 24). Recent studies have revealed an important role

**Conflict of interest:** The authors have declared that no conflict of interest exists.

**Copyright:** © 2021, American Society for Clinical Investigation.

**Submitted:** January 2, 2020; **Accepted:** January 22, 2021; **Published:** March 15, 2021.

**Reference information:** *J Clin Invest.* 2021;131(6):e136098.

<https://doi.org/10.1172/JCI136098>.

for N-cad in maintaining the quiescent status of NSCs (25, 26), and quiescence can confer radioresistance (6, 7). However, the role of N-cad in adaptive brain tumor radioresistance has not been investigated to date.

Here we examined the role of cell-cell adhesion and N-cad expression in adaptive radioresistance of GSCs and examined whether the resistance pathways could unveil new therapeutic approaches to resensitize radioresistant tumors.

## Results

*Radioresistant GSCs display increased cell-cell adhesion, slower proliferation, and an elevation of stemness properties.* To unveil mechanisms underlying therapeutic resistance in GBM, we generated mouse GSCs by transforming adult subventricular zone neural stem/progenitor cells through *Ink4a/Arf*<sup>-/-</sup> loss and activation of the ras pathway as occurs in human gliomas (27). The cells grow as spheres in stem cell medium, so we called them mouse glioma spheres (mGSs). We progressively adapted mGSs to irradiation in vitro by exposing them to 12 doses of 5 Gy (60 Gy total; see Methods). Comparison of parental (mGS) and radiation-adapted GSCs (mGSRRs) confirmed increased radioresistance of mGSRR cells in vitro (Figure 1A). To analyze their in vivo radioresistance, we stereotactically injected 1000 mGS or mGSRR cells into mice brains and performed repeated brain irradiation (2 Gy × 5 days) starting from day 3 after tumor cell implantation, when they already formed small tumors (Supplemental Figure 1; supplemental material available online with this article; <https://doi.org/10.1172/JCI136098DS1>). mGS cells form aggressive tumors that lead to demise of 90% of mice within 15 days. The tumors are sensitive to irradiation, which extends life span up to 25 days. In contrast, mGSRR form aggressive tumors that do not respond to radiation therapy as evidenced by loss of survival benefit (Figure 1B). These data demonstrate that in vitro adaptation of GSCs to irradiation translates to in vivo radioresistance, suggesting mGS/mGSRR cells are a good experimental model to study mechanisms underlying GSC adaptive radioresistance.

To initially establish whether defined cell properties segregate with adaptive radioresistance of GSCs, we compared the biological characteristics of mGS and mGSRR cells. We found that mGSRR cells grow slower than mGS cells (Figure 1C), and their slow proliferation is stable even after repeated passages (7 tested so far). mGSRR cells also display higher self-renewal ability as shown by sphere formation assays, which is an important characteristic of stem-like cells (Figure 1D). To further analyze their stemness we examined the expression level of neural stem cell and progenitor marker Olig2 and neuronal differentiation marker Tuj-1 in response to repeated irradiation. Olig2 expression gradually increased while expression of Tuj-1 decreased (Figure 1E; see complete unedited blots in the supplemental material). mGSRR cells also express higher CD109 (Supplemental Figure 2), a known GSC marker (28). These data indicate that during the adaptive process, where GSCs progressively become radioresistant upon repeated irradiation, they reduce their growth rate and increase their stemness properties.

We also observed that mGSRR cells form tightly packed spheres in 3D cell culture, while those of mGS cells remain much looser (Figure 1F), suggesting a difference in adhesion phenotype.

To analyze the level of cell-cell adhesion, we incubated single cells in culture medium in nonadhesive polypropylene tubes for 4 hours at 37°C, and then separated attached from nonattached cells by differential centrifugation. These analyses showed that mGSRR cells display a higher level of cell-cell adhesion (Figure 1G). These findings suggest that the progressive adaptation of GSCs to repeated irradiation is accompanied with an augmentation in their cell-cell adhesive properties.

*Fractionated irradiation increases N-cad expression in GSCs and N-cad drives the radioresistance phenotype.* To identify how GSC adhesive properties are altered following adaptive radioresistance, we used microarray analysis to compare gene expression between mGS and mGSRR cells, and identified 227 genes upregulated in mGSRR (Supplemental Figure 3A). Gene ontology analysis showed that gene sets related to cell adhesion were upregulated (Supplemental Figure 3B). A similar analysis on a published microarray data set of primary and recurrent GBM (29) identified 77 upregulated genes related to cell adhesion in recurrent samples (Supplemental Figure 3, C and D). We then focused on the expression level of cell-cell adhesion molecules known to play a role in neural stem cell maintenance (25, 26), as these are the presumed cells of origin for GSCs. We found that N-cad is gradually increased during repeated irradiation, while E-cadherin is decreased (Figure 2A). Immunofluorescence confirmed increased cell-surface N-cad expression in mGSRR cells (Figure 2B). To determine whether N-cad upregulation is also related to radioresistance in human GSCs, we established radioresistant populations of MGG4 cells (30, 31) and found that repeated irradiation also induced progressive N-cad elevation (Figure 2C).

To establish whether N-cad is simply a biomarker of aggressive growth or a genuine driver of the above radioresistance phenotype, we stably transfected mGS cells with an N-cad expression vector (Supplemental Figure 4A). We observed increases in cell-cell adhesion and self-renewal ability (Supplemental Figure 4, B and C), a reduction in cell proliferation (Supplemental Figure 4D), and enhanced radioresistance (Supplemental Figure 4E), akin to mGSRR. Similarly, when we stably increased N-cad expression in MGG4 cells, their stemness increased as seen by Olig2 and Tuj-1 markers (Figure 2D), their cell proliferation decreased (Figure 2E), and their self-renewal ability and radioresistance increased (Supplemental Figure 4F and Figure 2F).

To further investigate the importance of N-cad for radioresistance in human GBM, we analyzed its expression in 4 matching pairs of GBM patient-derived xenograft (PDX) models that we adapted to irradiation in vivo (2 Gy × 6 = 12 Gy total over 2 weeks, Figure 2G). The tumors were allowed to regrow and then passaged to the next set of mice and subjected to the same protocol of irradiation. This was repeated up to 6 times to develop the radiation-resistant models. In the resistant tumors of 2 of the models tested (JX39 and JX14), N-cad and Olig-2 expression increased, whereas Tuj-1 expression dropped (Figure 2H). These changes were not observed in the other 2 models (Supplemental Figure 5). These findings show that adaptation to irradiation can also be accompanied by N-cad increase in human GBM, while suggesting that other adaptive pathways may also exist.

To determine whether elevated N-cad expression relates to prognosis, we compared the outcomes of patients with GBM with

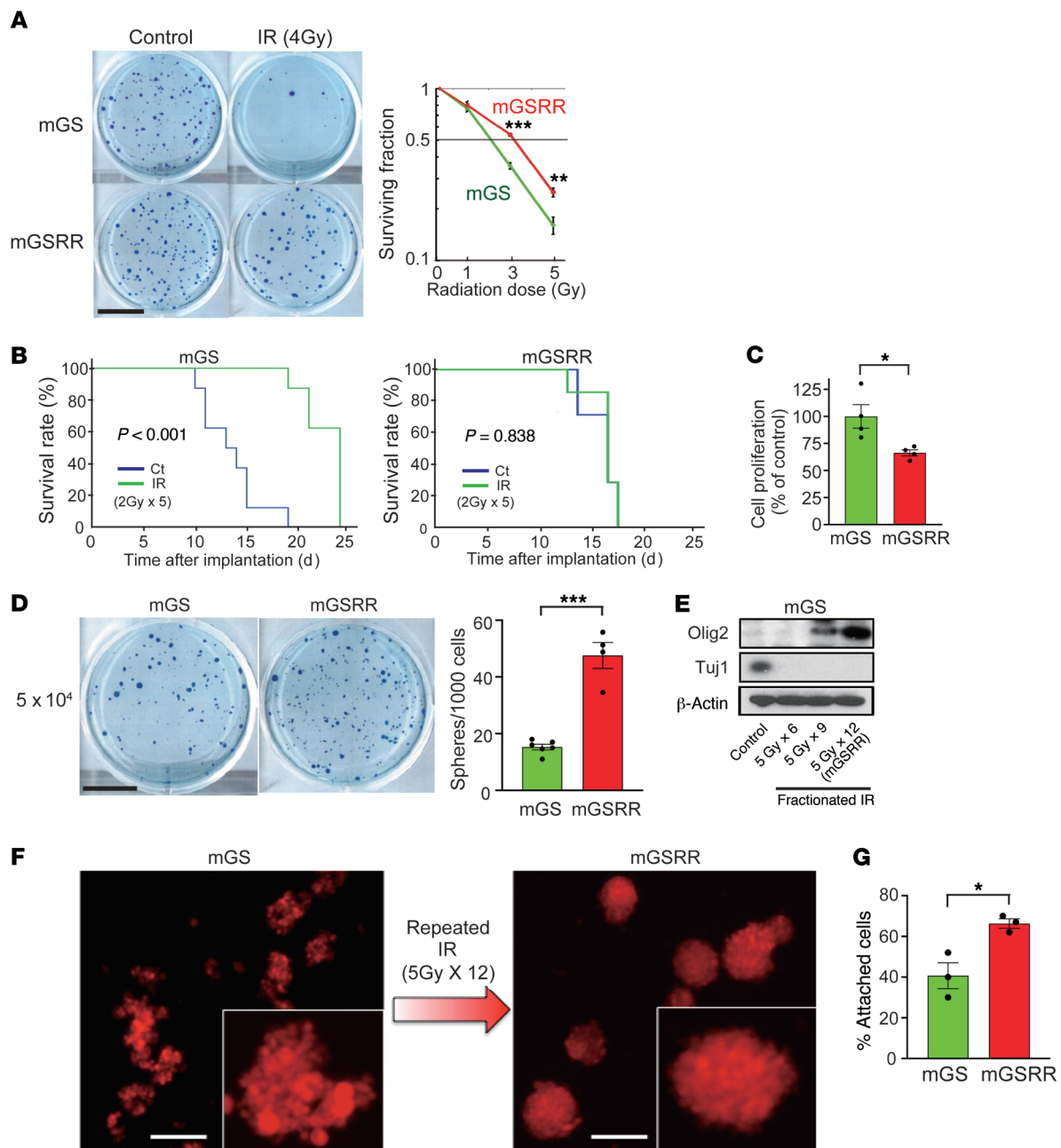


**Figure 1. Radioreistant GSCs display increased cell-cell adhesion, slower proliferation, and an elevation of stemness properties.** (A) Clonogenic survival assay for mGS and mGSRR subjected to irradiation (IR) or control without IR. Left: representative images of colonies formed by surviving cells 13 days after a single dose (4 Gy) of irradiation are shown. Right: fraction of surviving cells after radiation doses of 1, 3, or 5 Gy. Scale bar: 10 mm. (B) Survival curves for mice implanted with 1000 tumor cells (mGS or mGSRR) and subjected to whole-brain irradiation consisting of a daily dose of 2 Gy from days 3 to 7 after cell implantation (10 Gy total). Log-rank test. (C) Cell proliferation analysis for mGS and mGSRR after 72 hours. (D) Self-renewal ability of mGS and mGSRR as evaluated by sphere formation assay in soft agar. Scale bar: 10 mm. (E) Western blot showing expression of stem cell marker (Olig2) progressively increases and neural differentiation maker (Tuj1) is decreased following repeated cycles of irradiation in mGS cells. All blots show representative images ( $n = 3$ ). (F) Representative images of mGS and mGSRR cells stably expressing a fluorescence marker (mCherry) and grown as spheres in neural stem cell medium are shown. Scale bars: 200  $\mu$ m. (G) Single-cell suspension of mGS and mGSRR cells were cultured for 4 hours, and then the number of nonattached cells determined by differential centrifugation. \* $P < 0.05$ , \*\* $P < 0.01$ , \*\*\* $P < 0.001$ , 2-tailed Student's  $t$  tests unless otherwise indicated.

high or low N-cad mRNA. We analyzed the outcomes in TCGA data sets (32, 33) and found that N-cad expression associated with poor prognosis ( $P = 0.005$ ; Figure 2I). This correlation was retained even after removal of patients with well-understood determinants of survival (IDH-mut, MGMT methylation) ( $P = 0.028$ ). These data

indicate that elevated N-cad predicts poor outcome in patients with GBM, and may thus represent a therapeutic target.

Overall, these results indicate that N-cad upregulation accompanies mouse and human GSC adaptation to irradiation and is an important driver of adaptive radioresistance.

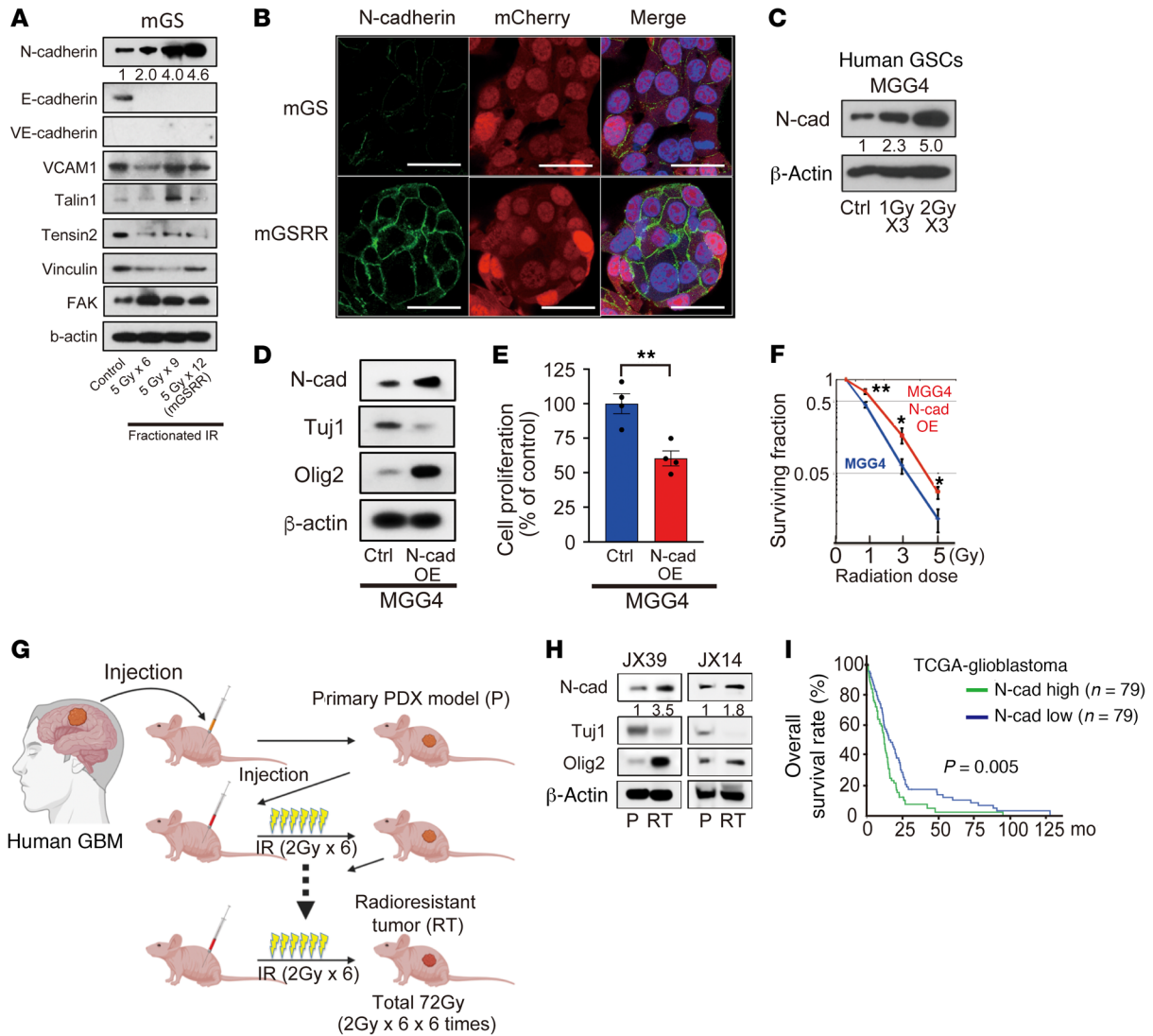


**Figure 2. Fractionated irradiation increases N-cad expression in GSCs and N-cad drives the radioresistance phenotype.** (A) Western blot showing expression of cell-cell adhesion molecules following 6 to 12 cycles of 5 Gy irradiation in mGS cells. (B) Fluorescence microscopy shows that N-cad expression is increased on the cell surface of mGSRR cells (green). mGS and mGSRR cells are stably expressing mCherry (red). Nuclei were counterstained with Hoechst 33342 (blue). Scale bars: 25  $\mu$ m. (C) Western blot showing expression of N-cad following 3 cycles of irradiation (1–2 Gy) in human GSCs, MGG4. (D) Western blot showing expression of N-cad, Tuj1, and Olig2 in human GSCs (MGG4) transfected with either control (Ctrl) or human N-cad expression vectors (OE). (E) Cell proliferation analysis for MGG4-Ctrl and MGG4 N-cad OE cells. (F) Clonogenic survival assay showing the surviving fraction of MGG4<sup>+/+</sup> N-cad cells after radiation doses of 1, 3, or 5 Gy. (G) Schematic showing experimental design to establish radioresistant PDX models. Subcutaneous tumors were exposed to repeated irradiation (2 Gy  $\times$  6 = 12 Gy total over 2 weeks). (H) Western blot showing expression of N-cad, Tuj1, and Olig2 in primary (P) or adapted to radiation therapy (RT) tumors of 2 PDX models. (I) Kaplan-Meier curve shows that increased N-cad mRNA expression is correlated with reduced survival in the TCGA-GBM data set. Log-rank test. High and low are defined as the top and bottom 15%. All blots show representative images ( $n = 3$  or more). \* $P < 0.05$ , \*\* $P < 0.01$ , 2-tailed Student's  $t$  tests unless otherwise indicated. The intensity of the immunoreactive bands was quantified in 3 independent experiments and the average is indicated below the blot.

*Knockout of N-cad in radioresistant GSCs annuls their radioresistance.* To further establish that N-cad is inherently linked to tumor formation and radioresistance of GSCs, we knocked out the *Cdh2* gene in mGS and mGSRR cells using the FokI/CRISPR/Cas9 system (34). We verified our N-cad knockout clones (mGS N-cad-KO #1 and #2, and mGSRR N-cad-KO) are devoid of N-cad protein (Figure 3A and Supplemental Figure 6A) due to clone-specific deletions that induce frameshifts (Supplemental Figure 6B). mGSRR N-cad-KO cells lost their ability to form tightly packed spheres (Figure 3B), grew faster than parental mGSRR cells

(Figure 3C), and had decreased self-renewal ability (Figure 3D), similar to mGS cells. As anticipated, these phenotypic changes were accompanied by decreased radioresistance in clonogenic survival assays (Supplemental Figure 6C). Similarly, N-cad knockout in mGS cells induced faster cell growth (Supplemental Figure 6D) and reduced survival rate (Supplemental Figure 6E).

To verify that our findings were not clonal artifacts, we reintroduced N-cad expression in mGS and mGSRR N-cad-KO cells (Figure 3, E and G). Similarly to mGS cells, N-cad-KO mGS cells formed aggressive tumors in mice brains. Also, irra-

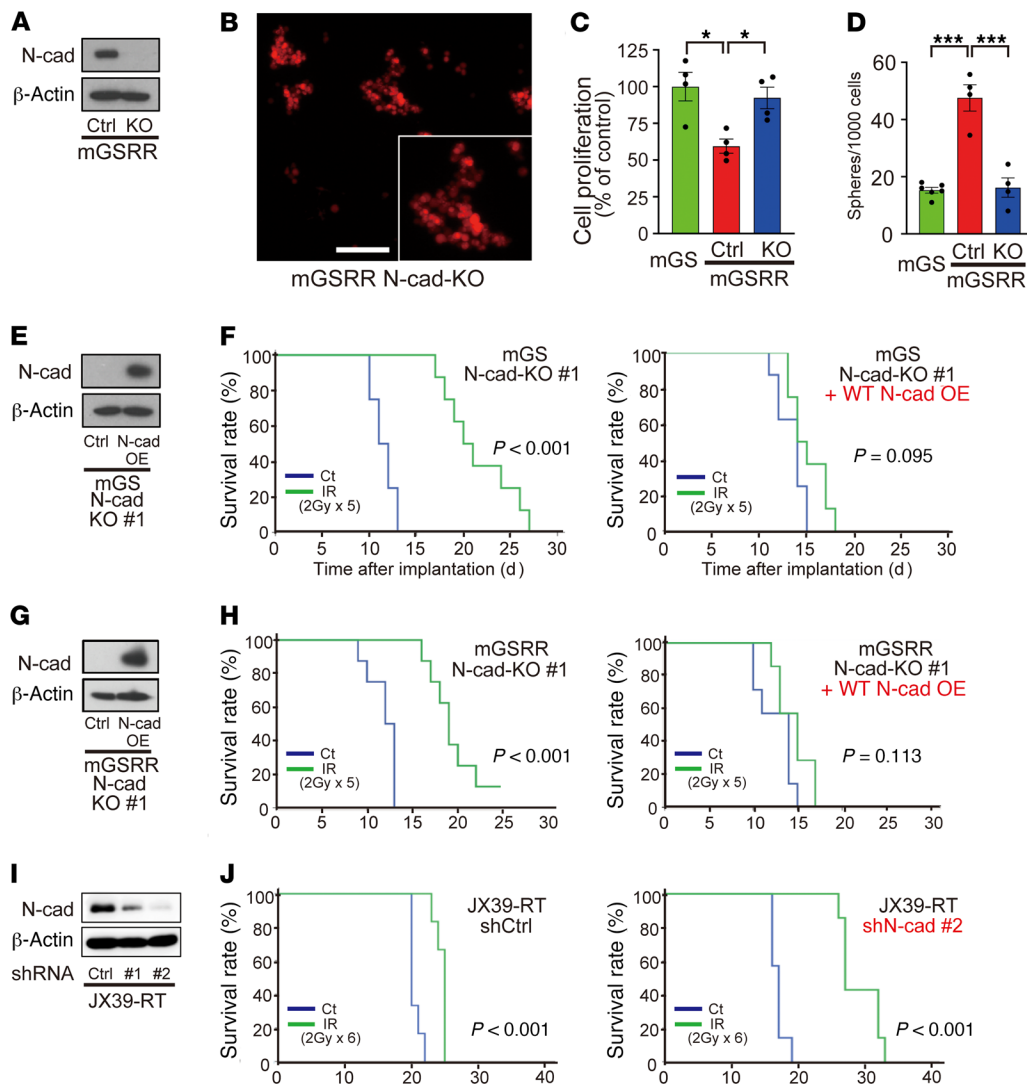


**Figure 3. Knockout of N-cad in radioresistant GSCs annuls their radioresistance.** (A) Western blot showing expression of N-cad in mGSRR and mGSRR with CRISPR/cas9-mediated knockout of *CDH2* (N-cad-KO). (B) Representative neurospheres of mGSRR N-cad-KO cells expressing a fluorescence marker (mCherry) grown in neural stem cell medium. Scale bar: 200  $\mu$ m. (C) Cell proliferation analysis for mGS, mGSRR, and mGSRR N-cad-KO cells after 72 hours.  $*P < 0.05$ , Tukey's HSD test. (D) Self-renewal ability of mGS, mGSRR, and mGSRR N-cad-KO as evaluated by sphere formation assay.  $***P < 0.001$ , Tukey's HSD test. (E) Western blot showing expression of N-cad in mGS N-cad-KO with or without N-cad restoration. (F) Survival curves for mice implanted with 1000 cells (mGS N-cad-KO with or without N-cad restoration) and subjected to whole-brain irradiation consisting of a daily dose of 2 Gy from days 3 to 7 after cell implantation (10 Gy total). Log-rank test. (G) Western blot showing expression of N-cad in mGSRR N-cad-KO cells with or without N-cad restoration. (H) Survival curves for mice implanted with 1000 cells (mGSRR N-cad-KO with or without N-cad restoration) and subjected to whole-brain irradiation (2 Gy  $\times$  5 days). Log-rank test. (I) Western blot showing expression of N-cad in JX39-RT cells transfected with control (Ctrl) or N-cad shRNAs (clones #1 and #2). (J) Survival curves for mice implanted with  $5 \times 10^5$  cells (JX39-RT with shCtrl or shN-cad #2) and subjected to whole-brain irradiation consisting of a dose of 2 Gy every other day over 2 weeks (12 Gy total). Log-rank test. All blots show representative images ( $n = 3$ ).

diation extended mice survival, showing tumor radiosensitivity (Figure 3F, left panel). Overexpression of N-cad eliminated the survival benefit, demonstrating that N-cad is sufficient to induce radioresistance (Figure 3F, right panel). Conversely, mGSRR cells devoid of N-cad lost their radioresistance, as evidenced by extended survival upon mice irradiation (Figure 3H, left panel). Exogenous restoration of N-cad eliminated the survival benefit, demonstrating restoration of radioresistance (Figure 3H, right panel).

To determine whether elevated N-cad expression also relates to radioresistance in hGSCs, we first established hGSCs from primary (JX39P) and adapted to radiation therapy (JX39RT) PDX

tumors by growing them in neural stem cell medium. We then stably transfected shRNA for N-cad in JX39RT GSCs and established 2 knockdown clones (Figure 3I). Clonogenic survival assays showed an increase in JX39RT colonies compared with parental JX39P, but their radioresistance was lost upon N-cad knockdown (Supplemental Figure 7, A and B). Radiation therapy had a modest effect (~25%) on survival time in mice injected with radioresistant JX39RT cells (shCtrl) while it increased survival by approximately 60% in mice harboring N-cad knockdown tumors (Figure 3J, compare left and right panels). These data show that N-cad can also induce in vivo radioresistance in human GSCs.

In sum, these results demonstrate that N-cad expression is dispensable for tumor formation but necessary for the maintenance of the radioresistance phenotype of GSCs, and that suppression of its expression leads to therapeutic radiosensitization.

*Single-cell analysis of human GBM heterogeneity reveals that N-cad expression associates with elevated stemness and low-proliferation gene expression signatures.* To evaluate whether a relationship exists between GSCs, N-cad expression, and rate of proliferation, we interrogated a data set (GSE57872) that contains individual gene expression profiles of single cells from human GBM (11). As expected, there was an inverse correlation between cells having elevated stemness or proliferation-related genes. Interestingly, N-cad levels correlated with the stem-like nature of the cells (Supplemental Figure 8), in agreement with our experimental findings that increased N-cad augments stemness in GSCs.

*Elevated N-cad increases cell-surface  $\beta$ -catenin, resulting in suppression of Wnt/ $\beta$ -catenin-mediated proliferative and neuronal differentiation signaling.* To start investigating the mechanisms underlying N-cad-mediated radioresistance in GSCs, we analyzed the expression levels of  $\beta$ -catenin,  $\alpha$ -catenin, and p120-catenin in mGS and mGSRR cells. N-cad has binding sites for  $\beta$ -catenin and p120-catenin, while  $\alpha$ -catenin is recruited to  $\beta$ -catenin once it is bound to N-cad (35, 36). Expression levels of  $\alpha$ -catenin and total and unphosphorylated  $\beta$ -catenin were gradually increased in response to repeated irradiation, in parallel with increased N-cad expression (Figure 4A). Free  $\beta$ -catenin is short-lived in the cytoplasm because of its immediate phosphorylation by the  $\beta$ -catenin destruction complex, which leads to degradation (35, 37). Hence, the accumulation of unphosphorylated  $\beta$ -catenin likely indicates that it binds to N-cad or accumulates in the nucleus. Using immunofluorescence, we found  $\beta$ -catenin accumulation at the cell surface, where N-cad is located (Figure 4B). Co-IP experiments also showed that N-cad binds to  $\beta$ -catenin (Supplemental Figure 9).

To evaluate whether N-cad-mediated trapping of  $\beta$ -catenin at the cell surface suppresses Wnt/ $\beta$ -catenin-mediated transcription, we used a TCF transcription factor-driven reporter. We found that radioresistant mGSRR cells have reduced Wnt/ $\beta$ -catenin transcriptional activity compared with mGS cells (Figure 4C). Consistently, Wnt/ $\beta$ -catenin transcriptional activity was suppressed by N-cad overexpression in mGS cells and increased upon N-cad knockout (Figure 4D). Consistently, mRNA expression of multiple Wnt/ $\beta$ -catenin target genes shown by microarray analysis was downregulated in mGSRR versus mGS cells (Figure 4E).

To determine whether reduced Wnt/ $\beta$ -catenin transcriptional activity underlies the higher stem-like phenotype in radioresistant GSCs, we probed expression of neural differentiation markers in mGS and mGSRR cells. Wnt-regulated master regulators for neuronal differentiation NeuroD1, Ngn1, and Brn3a (38, 39) were potently suppressed in mGSRR cells (Figure 4F). Similarly, overexpression of N-cad in mGS cells blocked Wnt signaling, as shown by stabilized  $\beta$ -catenin with low c-Myc expression and reduced expression of neural differentiation marker Tuj-1 (Figure 4G).

To further test whether the suppression of Wnt/ $\beta$ -catenin signaling augments radioresistance in GSCs, we analyzed the rate of surviving cells after treatment with 2 known Wnt acti-

vators by clonogenic survival assay. GSK3b inhibitors SB216763 and CHIR99021 both inhibited the phosphorylation of  $\beta$ -catenin within 2 hours after treatment (Supplemental Figure 10A) and reduced the radioresistance of mGSRR cells (Supplemental Figure 10, B and C).

In concert, these results indicate that upon elevation of N-cad expression, Wnt/ $\beta$ -catenin signaling is suppressed through trapping of  $\beta$ -catenin at the cell surface, preventing its nuclear translocation. This reduces Wnt/ $\beta$ -catenin target gene expression, which ultimately slows down GSC proliferation and suppresses their neuronal differentiation, resulting in reduced radioresistance.

*The CBR domain of N-cad is essential for radioresistance of GSCs.* To determine whether  $\beta$ -catenin binding to the intracellular C-terminus of N-cad is important for radioresistance in GSCs, we made an N-cad-expressing retroviral vector harboring a deletion in the  $\beta$ -catenin binding region ( $\Delta$ CBR, Figure 5A). We infected N-cad knockout mGS cells with WT- or  $\Delta$ CBR-N-cad-expressing viruses and measured their in vitro growth rate, stemness markers, and radioresistance. Restoration of WT but not  $\Delta$ CBR N-cad expression led to cell-surface accumulation and stabilization of  $\beta$ -catenin (Figure 5B), reduced expression of Wnt/ $\beta$ -catenin target c-Myc and neural differentiation marker Tuj-1, and increased neural stem/progenitor cell marker Olig2 (Figure 5C). Importantly, in contrast to WT-N-cad,  $\Delta$ CBR-N-cad failed to restore radioresistance (Figure 5D and Supplemental Figure 11). This may relate to incomplete suppression of TCF/ $\beta$ -catenin transcriptional activity (Figure 5E). Compared with WT-N-cad,  $\Delta$ CBR-N-cad only partially reduced cell proliferation (Figure 5F), which suggests that N-cad may regulate cell growth through both CBR-dependent and independent signaling. Overall, these results indicate that the binding between N-cad and  $\beta$ -catenin is important for the induction of radioresistance, slow growth, and stemness properties via Wnt/ $\beta$ -catenin signaling suppression.

*N-cad elevation increases Clusterin expression resulting in enhanced antiapoptosis function.* To further unveil the downstream effectors of N-cad-induced radioresistance, we performed RNA-seq analysis in 6 GSC pairs with or without elevated N-cad. We identified 9 genes consistently increased in N-cad-high GSCs and focused on *CLU*, which encodes Clusterin (Clu), as its expression most consistently related to N-cad status in all clones analyzed (Figure 6A). Alternative splicing can generate several Clu isoforms, but the main one functions as a multifunctional chaperone that confers antiapoptosis, cell growth, and metabolic changes in cancer cells (40–42). Our query of the Human Protein Atlas (43) evidenced Clu upregulation in several cancers including malignant glioma (data not shown). We confirmed Clu protein expression gradually increased during repeated irradiation in parallel with N-cad upregulation in both mouse and human GSCs (Figure 6, B and C). In mGS cells, N-cad knockout suppressed, while N-cad restoration increased Clu (Figure 6D). N-cad knockdown also reduced Clu expression in the human PDX line JX39RT (Figure 6E). Furthermore, examination of *CDH2* and *CLU* gene expression in the GBM TCGA data set showed a statistically significant correlation (Figure 6F).

Stable overexpression of Clu increased radioresistance in mGS cells, while shRNA-mediated knockdown decreased radio-

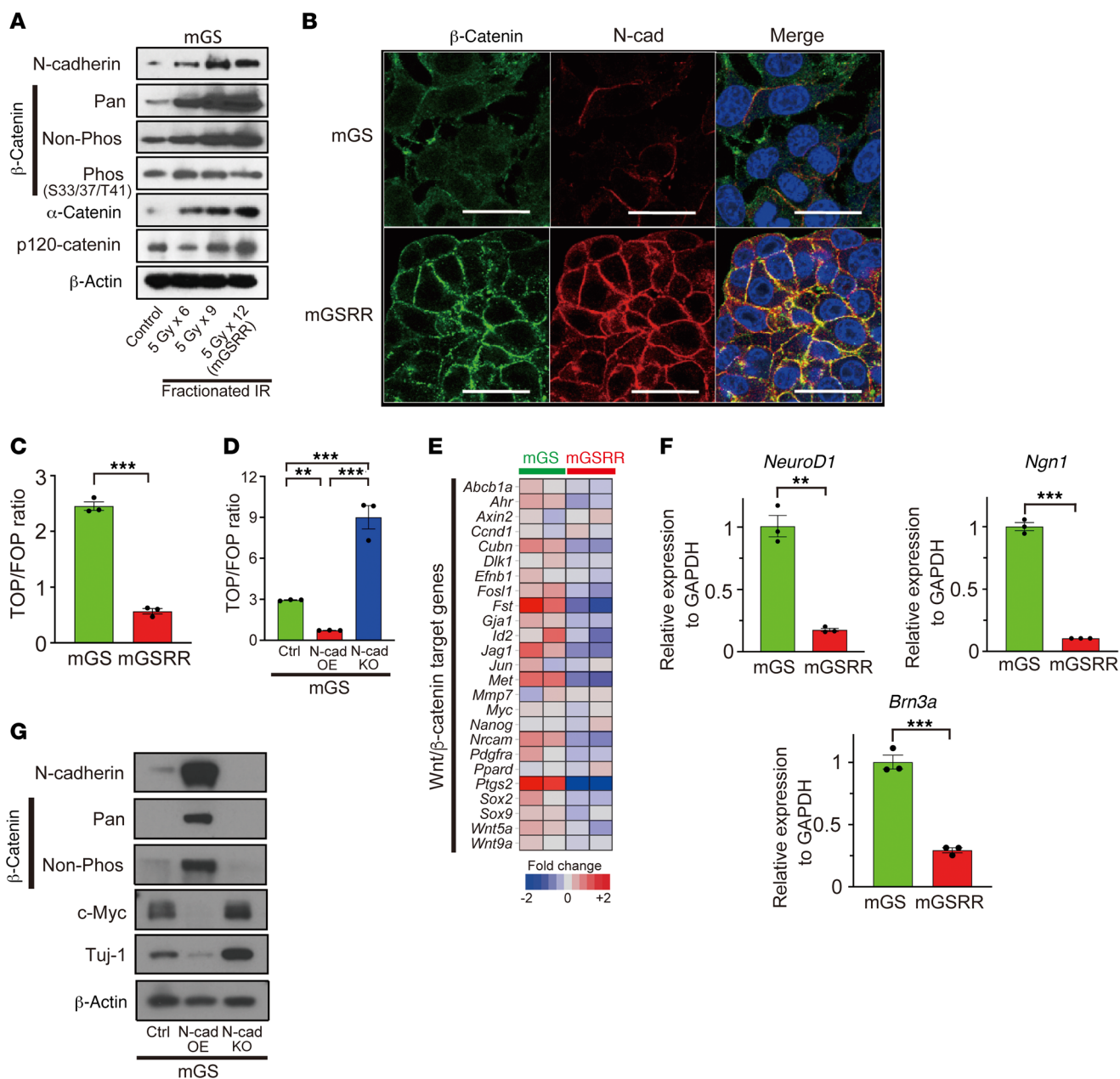


**Figure 4. Elevated N-cad leads to increased levels of cell-surface  $\beta$ -catenin, resulting in suppression of Wnt/ $\beta$ -catenin-mediated proliferative and neuronal differentiation signaling.** (A) Western blot showing expression changes of several N-cad binding catenins following 6–12 cycles of irradiation (5 Gy) in mGS cells. (B) Fluorescence microscopy shows that  $\beta$ -catenin (green) selectively coaccumulates with N-cad (red) on the cell surface of mGSRR but not mGS cells. Nuclei were counterstained with Hoechst 33342 (blue). Scale bars: 25  $\mu$ m. (C) Wnt/ $\beta$ -catenin regulated transcriptional activity in mGS and mGSRR cells measured through transient transfection with a luciferase reporter driven by a WT (TOP) or mutant (FOP) TCF binding site.  $***P < 0.001$ , 2-tailed Student's *t* test. (D) TOP/FOP ratio showing Wnt/ $\beta$ -catenin activity in parental N-cad-overexpressing and N-cad-KO mGS cells.  $***P < 0.01$ ,  $***P < 0.001$ , Tukey's HSD test. (E) Microarray analysis showing that mRNA expression of multiple Wnt target genes is suppressed in mGSRR compared with mGS cells. Each group contains 2 independent replicates ( $n = 2$ ). (F) qRT/PCR showing that *NeuroD1*, *Ngn1*, and *Brn3a* mRNAs are reduced in mGSRR cells. Two-tailed Student's *t* test. (G) Western blot showing expression change of  $\beta$ -catenin (pan and non-phospho), c-Myc, and Tuj1 by N-cad-overexpressing and N-cad-KO mGS cells. All blots show representative images ( $n = 3$  or more).

resistance in mGSRR cells (Figure 6G). We analyzed the levels of the secreted form of Clu in conditioned medium (CM), as it plays an important role in antiapoptosis in cancer cells (40–42). We found higher constitutive levels in CM of mGSRR compared with mGS, and Clu concentration further increased after radiation therapy (Figure 6H). Importantly, Clu secretion was dependent upon N-cad expression, as N-cad knockout abrogated it (Figure

6H). To determine whether Clu synthesis protects radioresistant GSCs against apoptosis, we exposed mGSRR cells to acute irradiation stress. Parental mGSRR cells were resistant to irradiation-induced PARP cleavage, while Clu knockdown and N-cad knockout sensitized the cells (Figure 6I). Next, we examined whether *CLU* gene expression related to patient survival, and found patients with GBM with high expression had statistically

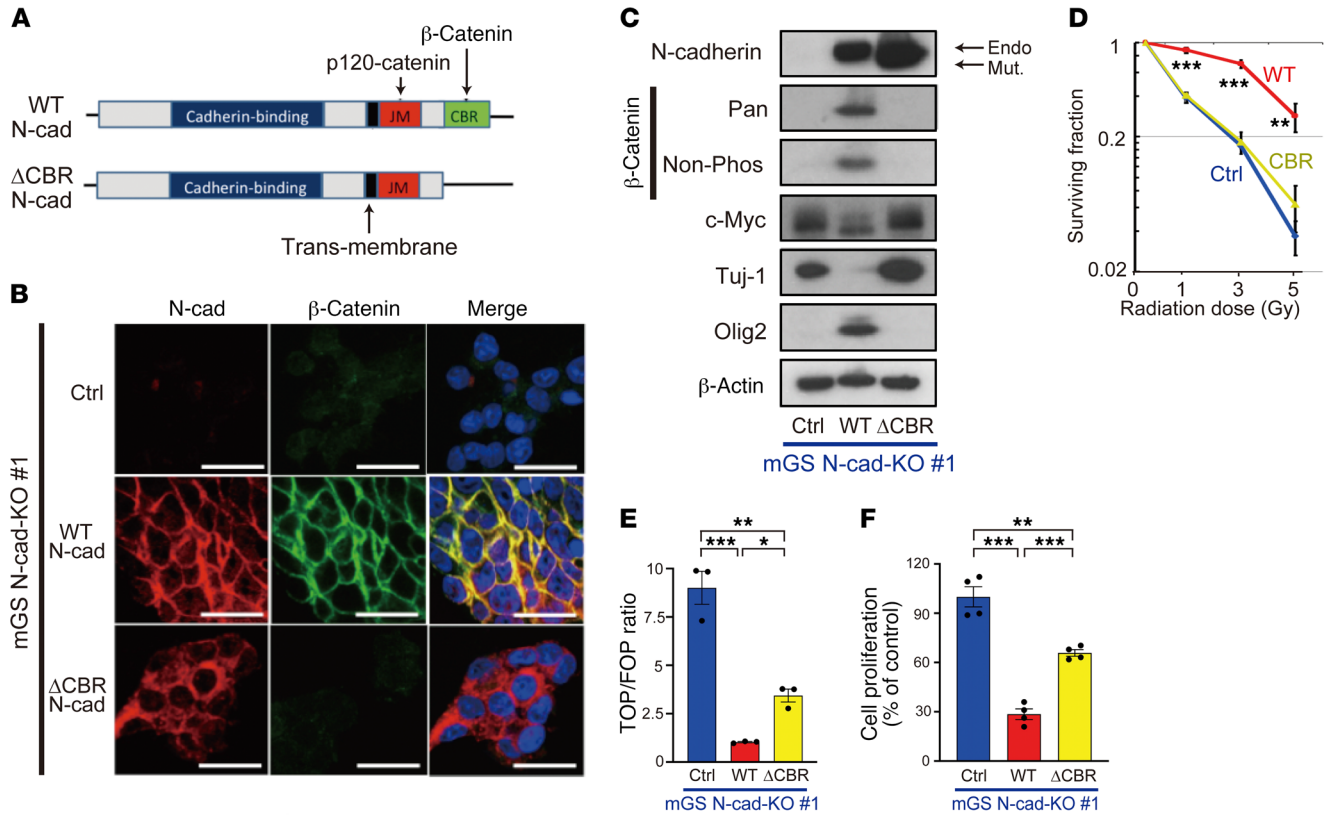


**Figure 5. The CBR domain of N-cad is essential for radioresistance of GSCs.** (A) Diagram showing expression vectors for N-cad WT and  $\Delta$ CBR, a mutant lacking the  $\beta$ -catenin binding region (CBR). JM, p120-catenin binding site. (B) Fluorescence microscopy shows that  $\beta$ -catenin accumulates at the cell surface of mGS N-cad-KO cells when reconstituted with WT N-cad, but not  $\Delta$ CBR N-cad. Nuclei were counterstained with Hoechst 33342 (blue). Scale bars: 25  $\mu$ m. (C) Western blot showing that restoration of WT but not  $\Delta$ CBR N-cad in GSCs knocked out for N-cad strongly stabilizes  $\beta$ -catenin expression, which reduces the expression of Wnt/ $\beta$ -catenin target genes c-Myc and neuronal marker Tuj-1. All blots show representative images ( $n = 3$ ). (D) Clonogenic survival assay shows reconstitution with WT, but not  $\Delta$ CBR N-cad increases survival in mGS-N-cad KO cells.  $***P < 0.001$ , Tukey's HSD test. (E) Wnt/ $\beta$ -catenin transcriptional activity (TOP/FOP luciferase reporter ratio) is strongly suppressed in mGS N-cad-KO cells when reconstituted with WT N-cad, but only partially with  $\Delta$ CBR N-cad.  $*P < 0.05$ ,  $**P < 0.01$ ,  $***P < 0.001$ , Tukey's HSD test. (F) Cell proliferation analysis for mGS N-cad-KO, with or without reconstitution with WT or  $\Delta$ CBR N-cad.  $**P < 0.01$ ,  $***P < 0.001$ , Tukey's HSD test.

worse outcomes (Figure 6J,  $P = 0.005$ ). Altogether, these results suggest that N-cad upregulates the synthesis and secretion of Clu, which confers radioresistance by protecting tumor cells from radiation-induced apoptosis.

*IGF-1 augments N-cad expression after radiation therapy.* To identify a potential point of intervention for therapy, we next focused on deciphering the upstream signaling underlying adaptive N-cad increase following repeated irradiation. RT-PCR revealed transcriptional reprogramming with an increase of N-cad and a concomitant decrease of E-cad mRNA expression in mGSRR (Figure 7A), a result reminiscent of an EMT-like transition. EMT is associated with radioresistance in epithelial cancers (44, 45), hence, we examined involvement of EMT master transcription factors. Snail1, Slug, and Zeb1 were gradually increased by repeated irradiation of mGS (Figure 7B). Congruently, microarray analysis indicated that expression of EMT target genes is increased in mGSRR cells compared with mGS cells (Supplemental Figure 12A). Similarly, analysis of a microarray data set (29) of human primary and recurrent GBM also showed that EMT target genes increase in recurrent radiotherapy-resistant GBM (Supplemental Figure 12B).

To further confirm that EMT-like reprogramming can induce N-cad upregulation and related radioresistance, we stably transfected Snail1 in mGS cells. Constitutive expression of Snail1 in mGS cells increased N-cad and Olig2 expression, reduced Tuj1 levels (Figure 7C), and led to a dramatic drop in TCF/ $\beta$ -catenin-driven transcription (Figure 7D), a phenotype reminiscent of mGSRR cells. Snail also rendered the cells as radioresistant as mGSRR cells (Figure 7E).

Therapeutic treatments, including irradiation, can induce changes in secreted growth factors (46–49), including IGF1 and TGF- $\beta$ , which can trigger EMT (6, 50, 51). We found that treatment of mGS cells with mouse rIGF1 (100 ng/mL; for 3 days) prominently increased the expression of N-cad and other EMT transcription factors, while mouse rTGF $\beta$ 1 (10 ng/mL; 3 days) had more modest effects (Figure 7F). Moreover, mGSRR cells display increased *Igf1* mRNA expression (Supplemental Figure 13). Therefore, to directly analyze the role of IGF1 in GSC radioresistance, we established mGS cells with IGF1 overexpression. The cells displayed elevation of N-cad, Zeb1, and  $\beta$ -catenin (Figure 7G), and gained in vivo radioresistance (Figure 7H). These findings suggest that IGF1 is one of the driving

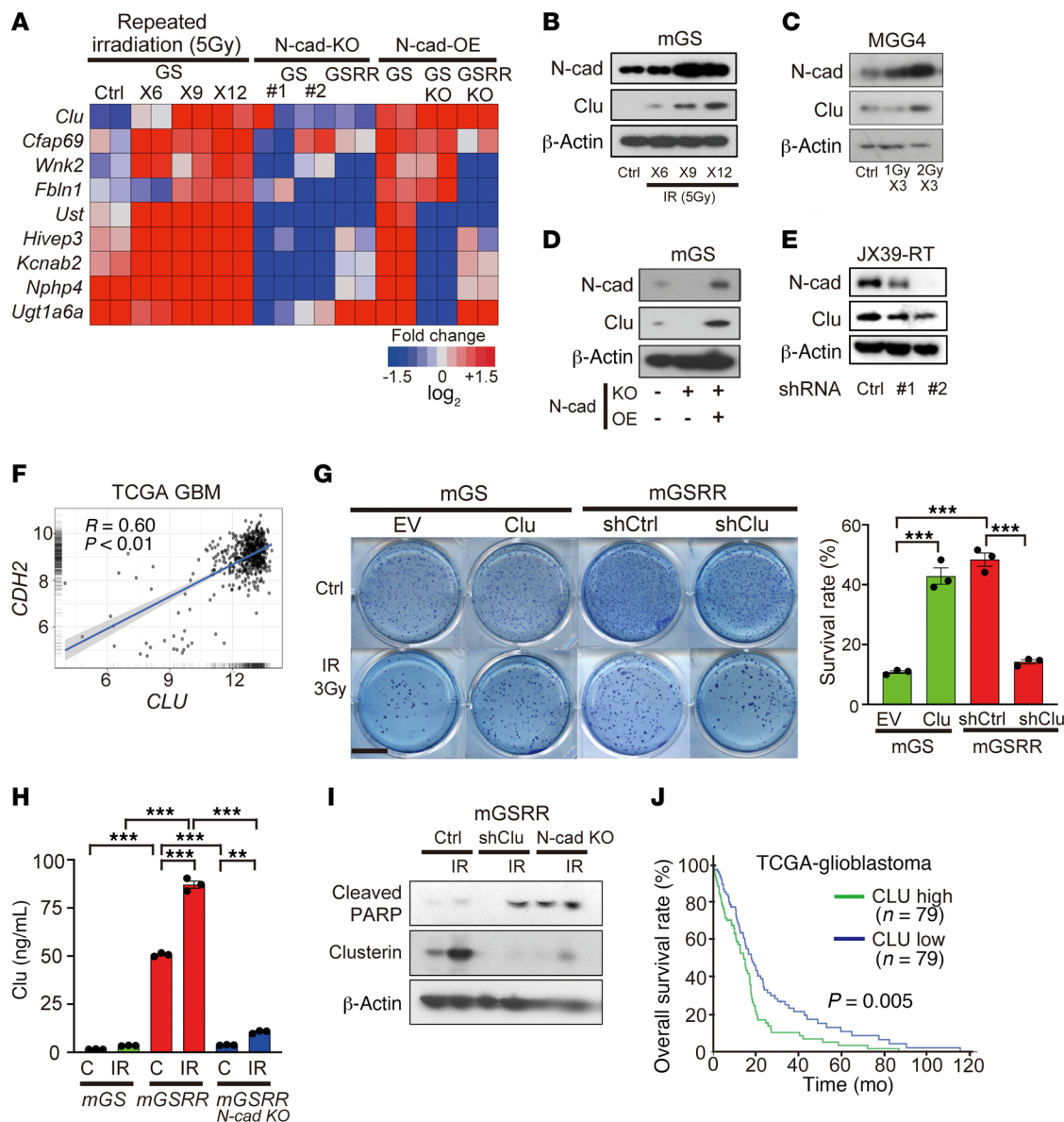


**Figure 6. Enhanced N-cad elevates Clusterin expression and protects against radiation-induced apoptosis.** (A) Heatmap comparing 9 gene mRNA expression measured by RNA-seq analysis in untreated mGS cells (Ctrl), in mGS cells after 6–12 cycles of fractionated irradiation with 5 Gy (Ct, 30 Gy, 45 Gy, and 60 Gy total dose), in mGS or mGSRR N-cad-KO cells (mGS N-cad-KO #1, #2, and mGSRR N-cad-KO), with or without N-cad reconstitution (OE). Two independent replicates per cell line ( $n = 2$ ). (B and C) Western blot showing expression of N-cad and Clu are gradually increased following mouse GS (B) and human MGG4 (C) adaptation to fractionated irradiation. (D) Western blot showing expression of Clu is suppressed by N-cad-KO and restored by stable N-cad transfection in mGS cells. (E) Western blot showing expression of Clu is suppressed by shRNA-mediated knockdown of N-cad in JX39-RT radioresistant PDX cells. (F) *CDH2* and *CLU* mRNA expression correlate in GBM (TCGA database). (G) Clonogenic survival assay for mGS cells transfected with control or Clu expression vectors and mGSRR cells transfected with shCtrl or shClu expression vectors with or without a single dose (3 Gy) of IR. Left: representative images of colonies formed by surviving cells 13 days after irradiation. Scale bar: 10 mm. Right: quantification of the fraction of surviving colony-forming cells.  $***P < 0.001$ , Tukey’s HSD test. (H) ELISA assay showing that Clu secretion is remarkably increased by mGSRR compared with mGS cells and this is strongly suppressed by N-cad knockout.  $**P < 0.01$ ,  $***P < 0.001$ , Tukey’s HSD test. (I) Western blot showing that suppression of Clu expression by shRNA or as a result of N-cad knockout increases PARP cleavage in mGSRR cells. (J) Kaplan-Meier curve shows that increased *CLU* mRNA expression is correlated with poor outcome in the TCGA-GBM data set. High and low are defined as top and bottom 15%. All blots show representative images ( $n = 3$ ).

growth factors that induce EMT and increase N-cad and radioresistance in GSCs.

Inhibitors of TGFβ1R and IGF1R are currently being tested in clinical trials, so we evaluated their efficacy in preventing N-cad-mediated acquired radioresistance in clonogenic survival assays (Figure 7I). We plated single mGS cells into 0.5%

agarose with or without inhibitors, performed repeated irradiation (4 Gy every 3 days; total 20 Gy), and counted the number of surviving colonies. These experiments revealed that approximately 14% of mGS cells survived the irradiation protocol (Figure 7I). To investigate how many of the resistant colonies had activation of the N-cad pathway, we isolated 12 individ-

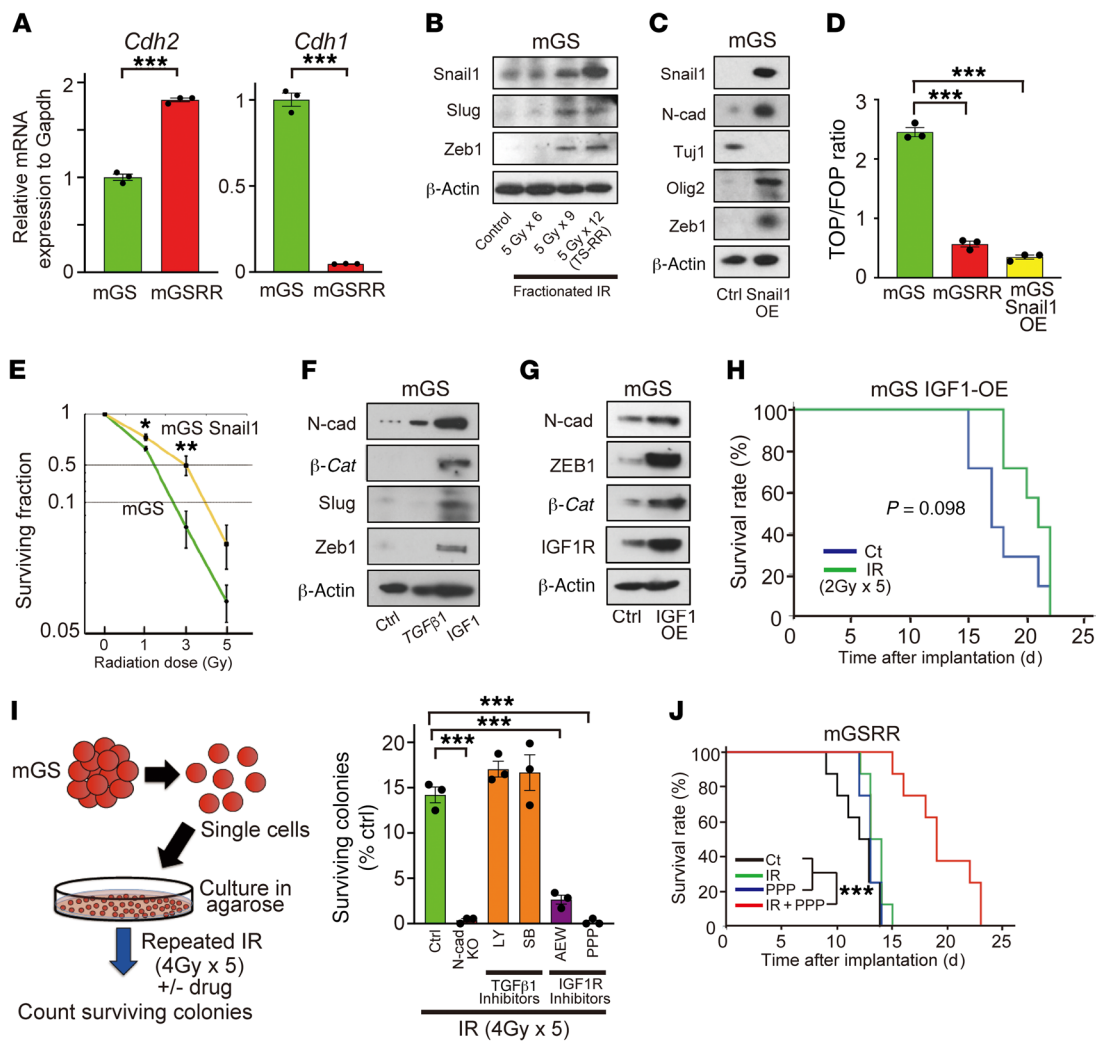


**Figure 7. IGF-1 augments N-cad expression after radiation therapy.** (A) qRT/PCR showing that mGSRR cells display increased *Cdh2* and decreased *Cdh1* mRNA expression compared with mGS. Two-tailed Student's *t* test. (B) Western blot showing expression of Slug, Snail1, and Zeb1 are gradually increased upon repeated irradiation in mGS cells. (C) Western blot showing that Snail overexpression induces elevation of N-cad, Olig2, and Zeb1, and suppression of TuJ1 in mGS cells. (D) Wnt/ $\beta$ -catenin transcriptional activity is suppressed in mGSRR and mGS with Snail1 overexpression (OE) compared with mGS cells. \*\*\* $P < 0.001$ , Tukey's HSD test. (E) Clonogenic survival assay shows mGS Snail1 OE cells have a higher survival rate than mGS cells. Two-tailed Student's *t* test. \* $P < 0.05$ , \*\* $P < 0.01$ . (F) Western blot showing increased N-cad,  $\beta$ -catenin, Slug, and Zeb1 expression 2 days after mouse recombinant IGF1 (100 ng/mL), but not TGF- $\beta$ 1 (10 ng/mL) treatment in mGS cells. (G) Western blot showing IGF1 overexpression increases N-cad,  $\beta$ -catenin, Zeb1, and IGF1R expression in mGS cells. (H) Survival curves for mice implanted with 1000 cells (GS with IGF1 expression vector) and subjected to whole-brain irradiation (2 Gy/day, days 3 to 7, 10 Gy total). (I) Left: schematic showing experimental design for clonogenic survival assay with repeated irradiation. Single mGS cells seeded in agarose medium were exposed to repeated irradiation (5 doses of 4 Gy, every 3 days) with or without drug rescue. IGF1R (AEW541 0.5  $\mu$ M; PPP 0.2  $\mu$ M) and TGF- $\beta$ 1 (LY2157299 10  $\mu$ M, SB431542 10  $\mu$ M) inhibitors were used. Right: quantification of percentage of surviving colonies shows that IGF1R inhibitors selectively decreased survival rate. Drugs alone had no effect on colony formation (data not shown). \*\*\* $P < 0.001$ , Dunnett's test. (J) Mice implanted orthotopically with mGSRR cells had a survival benefit after whole-brain irradiation (2 Gy x 5 days) with adjuvant PPP (15 mg/kg, i.p. twice a day from day 3-7) in contrast to vehicle control, only IR or PPP alone (8 mice/group; log-rank test). All blots show representative images ( $n = 3$  or more).

ual colonies and analyzed the expression level of N-cad and related signals. All clones displayed increased  $\beta$ -catenin levels, the majority of which had elevated Zeb1 and N-cad expression (Supplemental Figure 14). Consistently, knockout of N-cad in mGS led to less than 1% colonies, supporting a major role for N-cad in acquired radioresistance of GSCs (Figure 7I). Importantly, emergence of the adaptive resistance phenotype could be prevented, as inhibitors of IGF1 (AEW541 and picropodophyllin [PPP]) but not TGF $\beta$ 1 (LY2157299 and SB431542) sig-

naling almost completely abrogated resistant colony formation (Figure 7I;  $P < 0.001$ ). To determine whether IGF1R inhibitor effect depends on N-cad signaling, we performed colony survival assays with parental and N-cad knockout mGSRR cells after irradiation with or without PPP. PPP treatment reduced the number of surviving mGSRR colonies by approximately 80%, whereas it reduced GSR N-cad knockout colony formation by only 25% (Supplemental Figure 15). These data indicate that PPP mainly counteracts N-cad-mediated radioresistance,

but may also have ancillary effects. To determine whether these *in vitro* findings have therapeutic applicability in brain, we tested whether PPP, which is blood-brain barrier permeable (52), could resensitize radioresistant mGSR tumors to radiation therapy. Adjuvant PPP combined with irradiation potentially radiosensitized mGSR orthotopic mice xenografts and significantly extended mice survival versus irradiation only or drug alone controls (Figure 7J;  $P < 0.001$ ).

Altogether, these results suggest that N-cad upregulation was induced by radiation-induced IGF1 secretion and the radiation-resistance phenotype could be reverted with PPP, a clinically applicable blood-brain-barrier permeable IGF1 receptor inhibitor, supporting clinical translation.

## Discussion

In this study, we analyzed the adaptive radioresistance mechanisms induced in mouse and human GSCs during fractionated radiotherapy. We found that repeated GSC irradiation caused an increase in IGF1 secretion, leading to IGF1R-mediated intracellular EMT-like signaling and gradual upregulation of N-cad expression, which ultimately suppressed Wnt/ $\beta$ -catenin signaling by trapping  $\beta$ -catenin at the cell surface. This adaptation process switches the biological state of the cells toward increased cell-cell adhesion, augmented stemness and self-renewal capability, and reduced proliferation rate. Furthermore, N-cad upregulation also induced antiapoptotic signaling through an increase in secreted Clusterin. Antiproliferation and prosurvival signaling are known to confer radioprotection, explaining how through N-cad increase, GSCs can adapt and form highly radioresistant tumors.

Recurrent GBM is a highly radioresistant tumor that cannot be controlled by the highest dose (60 Gy) of fractionated radiation therapy safely tolerated by patients in clinical practice. To tackle this problem, a number of potential mechanisms driving radioresistance have been investigated (3, 53), but so far none have translated into novel effective therapies to increase radiosensitivity in patients. Recent genomic and molecular analyses have revealed that GBM is the most heterogeneous among all cancer types (54) and is composed of multiple tumor and inflammatory cell populations, including GSCs, which are more radioresistant than non-stem glioma cells. Prior studies have also suggested that GSCs initiate recurrence of tumors after standard therapy (6, 55).

Prior studies have revealed different mechanisms through which GSCs can maintain radioresistance, including increased DNA repair, antioxidative signaling, and antiapoptotic pathway activation (3, 55). Targeting of such pathways has shown promise in mouse models. However, none of these applications have so far succeeded in clinical trials, suggesting the existence of additional aspects of radioresistance that require further study. Our approach was to start with establishing radioresistance in human and mouse GSCs *in vitro* and focus on the resulting molecular alterations, which identified N-cad as a new driver of radioresistance. Rendering GSCs radioresistant is challenging due to their slow growth (6, 56, 57), and our study is the first to succeed in generating radioresistant human GSCs, which evidenced the same N-cad-dependent adaptive radioresistance pathway as that identified in mouse GSCs.

Our study reveals a major role for N-cad in establishing radioresistance in mouse and human GSCs and further shows that N-cad levels correlate with GBM patient survival. N-cad is a transmembrane protein and among the most important cell-cell adhesion molecules in the brain (19, 20). Glioma cells and GSCs express N-cad (21–23), which has a role in tumor invasion (23, 24). However, the role of N-cad as an effector of adaptive brain tumor radioresistance had not been investigated to date. We found that adaptation of GSCs to repeated irradiation occurs with stepwise increase in N-cad expression, which augments cell-cell adhesion and localization of  $\beta$ -catenin at the cell surface. Trapping of  $\beta$ -catenin by N-cad at the cell membrane stabilizes it, but at the same time prevents its nuclear translocation, explaining reduced TCF/ $\beta$ -catenin transcription, hindering c-Myc-driven proliferation, and preventing neural differentiation. Direct transfer of N-cad to sensitive GSCs could make them radioresistant. Knockout of N-cad rendered them sensitive, showing therapeutic potential. Altogether, these data indicate that N-cad is a driver of tumor resistance to radiation therapy, in part by maintaining the quiescent and stemness nature of GSCs, which has broad applicability in oncology (6, 7). Interestingly, recent studies on neural stem cells (NSCs), believed to be cells of origin for GSCs, have revealed an important role for N-cad in maintaining the quiescent status of NSCs (25, 26), suggesting that GSCs potentially hijack this mechanism toward radioresistance.

GSC radioresistance was accompanied by stabilization of  $\beta$ -catenin and gene reprogramming toward a quiescent and stemness state.  $\beta$ -catenin is a key effector of the canonical Wnt pathway (35), and Wnt/ $\beta$ -catenin signaling can control neural development, tumor growth, and invasion of GSCs (1, 3). Cadherin junctions mediate  $\beta$ -catenin function, and N-cad C-terminus binds to  $\beta$ -catenin,  $\alpha$ -catenin, and p120 catenin (35, 36, 58). Prior studies revealed that increased expression of N-cad leads to the accumulation of  $\beta$ -catenin at the cell surface, thereby reducing nuclear Wnt/ $\beta$ -catenin signaling (59, 60). Consequently, alteration in N-cad expression is expected to modify the expression of Wnt/ $\beta$ -catenin target genes that regulate the balance between stemness/differentiation and cell growth/death. Our studies demonstrate a new function for Wnt/ $\beta$ -catenin signaling as a rheostat modulating radioresistance of GSCs.

Clu is a multifunctional glycoprotein that is normally secreted in response to stress and regulates cell survival (40–42). Clu plays an important role in antiapoptosis signaling in cancer and is overexpressed in several cancers, including malignant glioma, based on the Human Protein Atlas (43). Our studies reveal a new role for Clu in GSC radioresistance and establish what we believe is a novel relationship between Clu and N-cad expression. We found that N-cad is a strong inducer of *CLU* transcription in GSCs, thereby inducing an antiapoptotic state through elevation in Clu secretion. This innovative finding provides a new avenue for targeting the N-cad/Clu survival signaling axis to reduce radioresistance in GBM. Clu inhibitors are now being analyzed in clinical trials and our study provides the rationale for testing them in conjunction with radiotherapy to prevent the emergence of resistance.

We found that in response to fractionated irradiation, GSCs produce increased amounts of IGF1, a growth factor that can induce EMT-like signaling, including upregulation of N-cad.

Moreover, we showed that antagonizing IGF1R signaling with PPP, a small molecule IGF1R inhibitor, reversed radioresistance. Overexpression of IGF1 and/or its receptor IGF1R has been reported in several cancers including glioblastoma, and IGF1R signaling is known to increase radio- and chemoresistance (6, 61–63), in part through Akt/Fox3a signaling (6). In the present study, we show that IGF1 is significantly involved in radioresistance via N-cad. Past clinical trials with tyrosine kinase receptor inhibitors (TKIs), including IGF1R inhibitors, have not resulted in remarkable success for reasons such as tumor cell heterogeneity, mutation of targeting site on receptor, or switch to alternative tyrosine kinase receptor signaling (64, 65). However, an appropriate design for clinical trials with IGF1R inhibitor PPP based on our findings could potentially lead to effective combination therapy with radiation for patients with GBM as it is BBB permeable. Prior trials using IGF1R inhibitors in patients with GBM showed their safety. However, they were only tested in recurrent patients, who do not receive radiation therapy. Our preclinical data in mice indicate that combination of IGF1R inhibitor and radiation therapy suppresses radioresistance of GSC-derived tumors, providing the rationale for new clinical trials in primary GBM.

In sum, our data reveal for the first time a role for N-cad-mediated cell-cell adhesion in the radioresistance of GSCs, thus connecting changes in mechanical properties with radiosensitivity. Our study deepens our understanding of adaptive radioresistance during repeated irradiation in GBM and validates the IGF/N-cad/ $\beta$ -catenin/Clu signaling axis as a novel target for radiosensitization, which has direct therapeutic applicability.

## Methods

**GSC generation and cell culture.** Mouse GSCs were generated by transforming adult subventricular zone-derived stem/progenitor cells from *Ink4a/Arf*<sup>-/-</sup> mice with human HRasV12 as previously described (6, 57), except that we used pMXs retroviral expression vector for H-ras, which yielded higher ras levels. The cells were subsequently implanted into the brains of wild-type C57BL/6J *Jms Slc* mice (Sankyo Labo Service Corporation), tumors harvested, and cells recovered and grown as mGS in neural stem cell medium (NSM). mGS cells form more aggressive gliomas in mouse brain than our previously described TS cells (6, 57), and 1000 implanted mGS cells kill mice within 15 days. Human primary GSC neurosphere cultures, MGG4 were provided by Hiroaki Wakimoto (Harvard University, Cambridge, Massachusetts, USA). Mouse and human GSCs were cultured in NSM, consisting of DMEM-F12 (MilliporeSigma, D8062) supplemented with recombinant human EGF (20 ng/mL) (PeproTech, AF-100-15), recombinant human bFGF (20 ng/mL) (PeproTech, 100-18B), B27 supplement without vitamin A (Invitrogen, 12587010), heparan sulfate (200 ng/mL, MilliporeSigma, H7640), penicillin, and streptomycin in a 5% CO<sub>2</sub> incubator at 37°C as described (66, 67). Cells were treated with recombinant mouse IGF1 (100 ng/mL, R&D Systems, #791-MG), recombinant mouse TGF- $\beta$ 1 (10 ng/mL, R&D Systems, #7666-MB), SB216763 (1–5  $\mu$ M, Selleckchem, S1075), or CHIR99021 (1–5  $\mu$ M, Selleckchem, S1263).

**Generation of radioresistant GSCs.** Radioresistant mouse and human GSCs were established by progressive adaptation to irradiation in vitro. Mouse GSCs were exposed to 5 Gy ionizing fractionated radiation every 3 to 4 days till 60 Gy total with the use of an x-irradiator (X-RAD 320; Accela) at settings of 320 kV and 10 mA as described (6).

Human GSCs were exposed to lower doses (1 or 2 Gy) of ionizing radiation every 4 to 7 days for a total dose of 3–6 Gy. The culture medium was replaced every 3 to 4 days, and the cells were passaged when confluent as needed.

**Radioresistant PDX model.** PDX were generated as previously described (68, 69). Briefly, primary PDX (JX14, JX39, 1153, and 1066) were established by growing patient-derived GBM subcutaneously in *nu/nu* mice. To establish radioresistant PDX, tumors grown subcutaneously in mice were exposed 3 times per week for 2 weeks to 2 Gy ionizing fractionated radiation (total 12 Gy). The tumors were then allowed to regrow, passaged to a new set of mice, and the same protocol of irradiation repeated (68). This was done up to 6 times to develop the radiation-resistant PDX models. hGSCs from primary and radioresistant PDX tumors were established by growing them in stem cell medium as previously described (6, 57).

**Generation of gene knockout cells with CRISPR/Cas9 system.** To knockout N-cad expression in mGS and mGSRR cells, the FokI CRISPR/Cas9 system was used (34). Multiplex gRNA expression plasmid (Addgene, pSQT1313, #53370) and FokI-dCas9 expression plasmid (pSQT1601, #53369) were provided by Keith Joung (Massachusetts General Hospital, Boston, Massachusetts, USA). We designed a guide RNA targeting the mouse *Cdh2* gene by using ZiFiT (<http://zifit.partners.org/ZiFiT/>) and cloned it into pSQT1313 as described (34). We targeted exon 5 because it encodes the first commonly used protein domain found in all splice variants of N-cad. We transfected the FokI-dCas9, guide RNA, and GFP expression plasmids into cells using Lipofectamine 3000 Transfection Reagent (Thermo Fisher Scientific, L3000001). We used FACS to isolate single cells expressing GFP, grew them into clones, and tested them for knockout of *Cdh2* expression using Western blotting and DNA sequencing.

**Cell transfection and viral vectors.** The following vectors were purchased from VectorBuilder: pMMLV-hCDH2 (human N-cadherin; NM\_001792.3), pMMLV-mCdh2 (mouse N-cadherin; ORF032915), pMMLV-mSnail1 (mouse Snail1; NM\_011427.2), pMMLV-mClu (mouse Clusterin; ORF041885), pLV-shCtrl-Puro, pLV-shCDH2 #1-Puro and pLV-shCDH2 #1-Puro. pMXs retroviral vector was provided by Toshio Kitamura (Institute of Medical Science, University of Tokyo, Tokyo, Japan) (70). Human IGF1 cDNA (NM\_00111285.3) was cloned into pMXs. Wild-type and mutant chicken N-cad expression vectors were gifted by Fumio Arai (Kyushu University, Fukuoka, Japan). All retroviral vectors were introduced into Plat-E (Cellbiolabs) or GP2-293 (Takara) packaging cells by transfection for 24 hours with the use of the Fugene HD reagent (Roche). The virus-containing culture supernatants were passed through a 0.45- $\mu$ m cellulose acetate filter, and the filtrate was collected for infection. Cells were seeded in 6-well dishes coated with poly-L-lysine (MilliporeSigma, P4707), infected, and subjected to selection with 10  $\mu$ g/mL puromycin (InvivoGen). The retroviral expression vector pSuper (OligoEngine) was used to introduce shRNA into cells. The sequences of the sense oligonucleotides were as follows: 5'-GGAGATTCAGAACGCCGTC-3' for mouse Clusterin shRNA and 5'-CGTACGCGGAATACTTCGA-3' for luciferase (nonspecific control) shRNA. The lentiviral expression vector pLV was used to introduce shRNA into JX39 cells. The sequences of the sense oligonucleotides were as follows: 5'-GGAACGCTGCAGATCTATTTA-3' (#1) and 5'-GTGCAACAGTATACGTTAATA-3' (#2) for human N-cadherin shRNAs and 5'-CCTAAGGTTAAGTCGCCCTCG-3' for scramble (nonspecific control) shRNA. Cells were infected with the

retroviral (71) and lentiviral (72) vectors as described and were then subjected to selection in the presence of puromycin as above.

**Cell-cell adhesion assays.** To analyze the level of cell-cell adhesion, we placed a suspension of single cells in culture medium ( $1 \times 10^5$  cells/mL) in nonadhesive polypropylene microfuge tubes and incubated them for 4 hours at 37°C without agitation, and then quantified the remaining number of nonattached cells by differential centrifugation. Percentage of attached cells was calculated as 1 minus the ratio of remaining nonattached cell density over initial cell density.

**Cell proliferation assays.** Cell proliferation was analyzed with the use of a WST-8 assay kit (Dojindo Laboratories) as described (6). Briefly, cells were plated at a density of  $4 \times 10^3$  per well in a 96-well plate and incubated in NSM for 48 or 72 hours, after which WST-8 reagents were added accordingly.

**Sphere formation assays.** Sphere formation assays were performed as described (6). Briefly, single cells were suspended in 0.5% agarose to prevent aggregation and plated in 6-well plates. The solidified cell layer was then covered with NSM and the medium was changed every 3 to 4 days. At 2 weeks (mGSCs) or 4 to 5 weeks (hGSCs) after plating, cells were fixed with 4% paraformaldehyde and stained with toluidine blue O (MilliporeSigma, T3260). The wells were photographed and spheres containing more than 100 cells were counted manually.

**3D Clonogenic survival assays to measure radioresistance.** Cells were embedded in 0.5% agarose as for the sphere formation assay, but at densities adjusted to result in a number of colonies approximately equal to that formed by the control group after 2 weeks (mGSCs) or 4 weeks (hGSCs). Twenty-four hours later, the cells were subjected to irradiation and returned to the incubator with medium changes every 3 to 4 days. Colonies were stained and counted after 2 weeks (mGSCs) or 4 to 5 weeks (hGSCs) as described above. To evaluate the radio-sensitivity for repeated irradiation in vitro (Figure 7I), we performed additional repeated irradiation (4 Gy  $\times$  5, 3-day interval) for cells surviving after single dose of irradiation. Culture medium was replaced every 3 days. IGF1R inhibitors PPP (0.2  $\mu$ M, Santa Cruz, sc-204008) and AEW541 (0.5  $\mu$ M, Active Biochemicals, A-1911), or TGF- $\beta$ 1 signaling inhibitor LY2157299 (10  $\mu$ M, Santa Cruz, sc-391123A), and SB431542 (10  $\mu$ M, Selleckchem, S1067) were added into the medium 24 hours before irradiation.

**Immunofluorescence.** Cells were cultured on glass-bottom plates (ibidi, #81506) coated with Matrigel (Becton Dickinson, 356234). GSCs were fixed with 4% paraformaldehyde for 10 minutes, and then permeabilized with 1% Triton X-100 for 10 minutes, blocked with 3% BSA in PBS for 1 hour, and incubated overnight with anti-mouse N-cadherin antibody (1:500, Becton Dickinson, 610920) or anti- $\beta$ -catenin antibody (1:500, Cell Signaling, #8480). Cells were examined using a confocal microscope (Leica, SP-8). Nuclei were counterstained with Hoechst 33342 (Invitrogen, H3570).

**Western blot.** Western blots were performed as described (73) using antibodies targeting the following proteins: Olig2 (1:1000, Millipore, AB9610), Tuj1 (1:1000, Biolegend, 801202),  $\beta$ -actin (1:2000, Santa Cruz, sc-69879), CD109 (1:100, Santa Cruz, sc-271085), mouse N-cadherin (1:500, Becton Dickinson, 610920), human N-cadherin (1:500, Santa Cruz, sc-7939), E-cadherin (1:1000, Cell Signaling, #3195), VE-cadherin (1:500, Santa Cruz, sc-9989), VCAM1 (1:250, Santa Cruz, sc-8304), Talin1 (1:500, Cell Signaling, #4021), Tensin2 (1:500, Cell Signaling, #11990), Vinculin (1:500, Cell Signaling, #4650), FAK (1:500, Cell Signaling, #3285),  $\beta$ -catenin (1:500,

Becton Dickinson, #610193), pan  $\beta$ -catenin (1:500, Cell Signaling, #8480), non-phospho  $\beta$ -catenin (1:500, Cell Signaling, #8814), phospho- (S33/S37/T41)  $\beta$ -catenin (1:500, Cell Signaling, #9561), p120-catenin (1:500, Becton Dickinson, 610133), c-Myc (1:1000, Cell Signaling, #5605), cleaved PARP (1:500, Cell Signaling, #9544), mouse Clusterin (1:500, R&D, AF2747), human Clusterin (1:500, Santa Cruz, sc-5289), Snail1 (1:500, Cell Signaling, #3879), Slug (1:500, Cell Signaling, #9585), Zeb1 (1:1000, Cell Signaling, #3396), and IGF1R (1:500, Cell Signaling, #3018). Coimmunoprecipitation experiments were performed with a Dynabeads protein A immunoprecipitation kit (Invitrogen, 100006D).

**WNT/ $\beta$ -catenin reporter assays.** Luciferase reporter gene transfections were performed with lipofectamine using a reporter gene construct driven by a TCF binding site (M50 Super 8x TOP Flash, Addgene, #12456) and a negative control with a mutant TCF binding site (M51 Super 8x FOP Flash, Addgene, #12457), which were provided by Randall Moon (University of Washington, Seattle, Washington, USA). After 48 hours, cells were lysed and luciferase activity was quantified with the Dual-Luciferase Reporter Assay System (Promega).

**Radiation cell survival assays.** Cells were plated at a density of  $4 \times 10^3$  per well in a 96-well plate 24 hours before irradiation (5 Gy). After 48 hours, WST-8 reagents were added according to the manufacturer's instructions.

**Animal experiments.** Orthotopic implantation of cells was performed as described (6, 57). For radiation experiments, 1000 viable mouse GSCs or 500,000 viable human GSCs were injected into the right forebrain of C57BL/6 mice (Charles River, age 5–6 weeks, female) or homozygous outbred athymic nude mice (J:NU, Jackson Laboratories, stock no: 007850, age 5–6 weeks, female). The animals received daily whole-brain irradiation (2 Gy) from days 3 to 7 after mGSC implantation. For hGSCs, the mice received a total 12 Gy radiation (from day 3, 2 Gy/day, every other day, 3 times per week for 2 weeks). Radiation was confined to the brain by protection of the body with a lead shield. Mice were observed daily and killed when moribund. PPP (15 mg/kg, Santa Cruz, sc-204008) was injected i.p. twice a day from days 3 to 7 in an aqueous solution containing 0.9% DMSO (MilliporeSigma), 7% *N*-dimethylacetamide (MilliporeSigma), and 10% Cremophor EL (MilliporeSigma). Control mice were treated with vehicle only. Tumor size at irradiation start time was estimated by bioluminescence imaging (IVIS Spectrum, PerkinElmer).

**Bioinformatics.** We performed microarray and RNA-seq analyses on mouse GSCs as described (74). Published microarray data including 70 primary GBM and 10 recurrent GBM were obtained from GEO data set GSE7696 (29) and analyzed as described (74). Briefly, raw expression data (CEL files) were summarized and normalized using the Robust Multi-array Average algorithm and the Bioconductor package affy (<http://www.bioconductor.org/packages/2.0/bioc/html/affy.html>). The Cancer Genome Atlas (TCGA) GBM data set was analyzed using GlioVis (<http://gliovis.bioinfo.cnio.es>). To perform RNA-seq analysis of single cells from primary GBM we used GEO data set GSE57872 (11). The Spotfire software package (TIBCO Software) was used to generate a heatmap with sample values.

**qRT-PCR.** We performed real-time quantitative reverse transcription PCR (qRT-PCR) as described (75). Briefly, total RNA was isolated using the RNeasy Mini Kit (Qiagen). Reverse transcriptase

reaction was performed with PrimeScript RT reagent kit with gDNA eraser (Takara) according to the manufacturer's instructions. qRT-PCR was performed in triplicate using SYBR Green reagent (Applied Biosystems). *Gapdh* qRT-PCR was set as an internal control. The following primer sets were used: *NeuroD1* (5'-AAGCCATGAATG-CAGAGGAGGACT, 5'-AGCTGCAGGCAGCCGGCGACC), *Ngn1* (5'-TCGGCTTCAGAAGACTTCAC, 5'-GTGGTATGGGATGAAA-CAGG), *Brn3a* (5'-CTCACGCTCTCGCACAAAC, 5'-AGAGCTCCG-GCTTGTTCAT), *Cdh1* (5'-TTGAGGCCAAGCAGCAATACATCC, 5'-AGATGTGATTTCTGACCCACACC), *Cdh2* (5'-TTGCTTCTG-ACAATGGAATCCCGC, 5'-AAGGAAAGATCAAACGCGAACGGC), *Gapdh* (5'-GTGAAGTCCGGTGTGAACG, 5'-GACCATGTAGTT-GAGGTCAATG), and for *Igf1* (5'-CTACAAAAGCAGCCCGCTCT, 5'-CTTCTGAGTCTTGGGCATGTCA).

**Statistics.** Results were analyzed using 2-tailed Student's *t* test, Tukey's HSD test, Dunnett's test, 2-way ANOVA, or the Mann-Whitney *U* test in IBM SPSS Statistics 18 software to assess statistical significance. Kaplan-Meier survival analyses were performed using the log-rank test. *P* less than 0.05 was considered statistically significant. Data were graphed as mean  $\pm$  SEM.

**Study approval.** Animal studies were performed with approval by the IACUC of Emory University or the University of Alabama at Birmingham. The collection of human samples was performed through IRB-approved protocols at Emory University or the University of Alabama at Birmingham.

## Author contributions

SO performed most of the experiments. DZ constructed expression vectors. CL and ZZ performed the stereotactic neurosurgery. JJO provided advice. CTS, GYG, and CDW provided the radioresistant PDX models. OS and HS provided established mouse GSCs. SO and EGVM conceived the project, designed experiments, and wrote the manuscript.

## Acknowledgments

We thank Narra Sarojini Devi and Svetlana Komarova for technical support. We appreciate the helpful advice and assistance of all members of our laboratory. Illustrations were created with BioRender (<https://biorender.com/>). This work was supported in part by grants from the NIH (CA163722, NS096236, and NS117666 to EGVM; CA223976 to GYG and CDW, and P30 CA013148 to the O'Neal Comprehensive Cancer Center), the Department of Defense (CA170948 to EGVM), the Southeastern Brain Tumor Foundation (to EGVM and SO), and the Japan Society for the Promotion of Science (26830082 and 13J06657 to SO).

Address correspondence to: Erwin G. Van Meir or Satoru Osuka, O'Neal Comprehensive Cancer Center, University of Alabama at Birmingham, 1720 2nd Avenue South, Birmingham, Alabama 35294, USA. Phone: 205.975.0694; Email: [evanmeir@uab.edu](mailto:evanmeir@uab.edu) (EGVM). Phone: 205.975.5973; Email: [sosuka@uabmc.edu](mailto:sosuka@uabmc.edu) (SO).

- Schonberg DL, et al. Brain tumor stem cells: Molecular characteristics and their impact on therapy. *Mol Aspects Med.* 2014;39:82-101.
- Hadjipanayis CG, Van Meir EG. Brain cancer propagating cells: biology, genetics and targeted therapies. *Trends Mol Med.* 2009;15(11):519-530.
- Lathia JD, et al. Cancer stem cells in glioblastoma. *Genes Dev.* 2015;29(12):1203-1217.
- Skvortsova I, et al. Radiation resistance: cancer stem cells (CSCs) and their enigmatic pro-survival signaling. *Semin Cancer Biol.* 2015;35:39-44.
- Vogin G, Foray N. The law of Bergonié and Tribondeau: a nice formula for a first approximation. *Int J Radiat Biol.* 2013;89(1):2-8.
- Osuka S, et al. IGF1 receptor signaling regulates adaptive radioprotection in glioma stem cells. *Stem Cells.* 2013;31(4):627-640.
- Lu D, et al. Fra-1 promotes breast cancer chemosensitivity by driving cancer stem cells from dormancy. *Cancer Res.* 2012;72(14):3451-3456.
- Wang Y-Z, et al. Concise review: quiescent and active states of endogenous adult neural stem cells: identification and characterization. *Stem Cells.* 2011;29(6):907-912.
- Boulais PE, Frenette PS. Making sense of hematopoietic stem cell niches. *Blood.* 2015;125(17):2621-2629.
- Zhu Z, et al. Targeting self-renewal in high-grade brain tumors leads to loss of brain tumor stem cells and prolonged survival. *Cell Stem Cell.* 2014;15(2):185-198.
- Patel AP, et al. Single-cell RNA-seq highlights intratumoral heterogeneity in primary glioblastoma. *Science.* 2014;344(6190):1396-1401.
- Eke I, Cordes N. Focal adhesion signaling and therapy resistance in cancer. *Semin Cancer Biol.* 2015;31:65-75.
- Farahani E, et al. Cell adhesion molecules and their relation to (cancer) cell stemness. *Carcinogenesis.* 2014;35(4):747-759.
- Redmer T, et al. E-cadherin is crucial for embryonic stem cell pluripotency and can replace OCT4 during somatic cell reprogramming. *EMBO Rep.* 2011;12(7):720-726.
- Martino G, Pluchino S. The therapeutic potential of neural stem cells. *Nat Rev Neurosci.* 2006;7(5):395-406.
- Machon O, et al. Role of beta-catenin in the developing cortical and hippocampal neuroepithelium. *Neuroscience.* 2003;122(1):129-143.
- Takashima Y, et al. Promising prognosis marker candidates on the status of epithelial-mesenchymal transition and glioma stem cells in glioblastoma. *Cells.* 2019;8(11):1312.
- Kim S-H, et al. Serine/threonine kinase MLK4 determines mesenchymal identity in glioma stem cells in an NF- $\kappa$ B-dependent manner. *Cancer Cell.* 2016;29(2):201-213.
- Hatta K, et al. A monoclonal antibody disrupting calcium-dependent cell-cell adhesion of brain tissues: possible role of its target antigen in animal pattern formation. *Proc Natl Acad Sci U S A.* 1985;82(9):2789-2793.
- Inuzuka H, et al. Differential expression of R- and N-cadherin in neural and mesodermal tissues during early chicken development. *Development.* 1991;113(3):959-967.
- Asano K, et al. Correlation of N-cadherin expression in high grade gliomas with tissue invasion. *J Neurooncol.* 2004;70(1):3-15.
- Shinoura N, et al. Expression of N-cadherin and alpha-catenin in astrocytomas and glioblastomas. *Br J Cancer.* 1995;72(3):627-633.
- Velpula KK, et al. Glioma stem cell invasion through regulation of the interconnected ERK, integrin  $\alpha$ 6 and N-cadherin signaling pathway. *Cell Signal.* 2012;24(11):2076-2084.
- Camand E, et al. N-cadherin expression level modulates integrin-mediated polarity and strongly impacts on the speed and directionality of glial cell migration. *J Cell Sci.* 2012;125(Pt4):844-857.
- Porlan E, et al. MT5-MMP regulates adult neural stem cell functional quiescence through the cleavage of N-cadherin. *Nat Cell Biol.* 2014;16(7):629-638.
- Miyamoto Y, et al. N-cadherin-based adherens junction regulates the maintenance, proliferation, and differentiation of neural progenitor cells during development. *Cell Adh Migr.* 2015;9(3):183-192.
- TCGA Network. Comprehensive genomic characterization defines human glioblastoma genes and core pathways. *Nature.* 2008;455(7216):1061-1068.
- Minata M, et al. Phenotypic plasticity of invasive edge glioma stem-like cells in response to ionizing radiation. *Cell Rep.* 2019;26(7):1893-1905.
- Murat A, et al. Stem cell-related "self-renewal" signature and high epidermal growth factor receptor expression associated with resistance to concomitant chemoradiotherapy in glioblastoma. *J Clin Oncol.* 2008;26(18):3015-3024.
- Wakimoto H, et al. Maintenance of primary tumor phenotype and genotype in glioblastoma stem cells. *Neuro Oncol.* 2012;14(2):132-144.
- Rheinbay E, et al. An aberrant transcription factor network essential for Wnt signaling and

- stem cell maintenance in glioblastoma. *Cell Rep.* 2013;3(5):1567–1579.
32. Brennan CW, et al. The somatic genomic landscape of glioblastoma. *Cell.* 2013;157(3):462–477.
  33. Nutt CL, et al. Gene expression-based classification of malignant gliomas correlates better with survival than histological classification. *Cancer Res.* 2003;63(7):1602–1607.
  34. Tsai SQ, et al. Dimeric CRISPR RNA-guided FokI nucleases for highly specific genome editing. *Nat Biotechnol.* 2014;32(6):569–576.
  35. Valenta T, et al. The many faces and functions of  $\beta$ -catenin. *EMBO J.* 2012;31(12):2714–2736.
  36. van Roy F. Beyond E-cadherin: roles of other cadherin superfamily members in cancer. *Nat Rev Cancer.* 2014;14(2):121–134.
  37. Liu C, et al. Control of beta-catenin phosphorylation/degradation by a dual-kinase mechanism. *Cell.* 2002;108(6):837–847.
  38. Kuwabara T, et al. Wnt-mediated activation of NeuroD1 and retro-elements during adult neurogenesis. *Nat Neurosci.* 2009;12(9):1097–1105.
  39. Rampazzo E, et al. Wnt activation promotes neuronal differentiation of glioblastoma. *Cell Death Dis.* 2013;4(2):e500.
  40. Zoubeidi A, et al. Targeting the cytoprotective chaperone, clusterin, for treatment of advanced cancer. *Clin Cancer Res.* 2010;16(4):1088–1093.
  41. Garcia-Aranda M, et al. Clusterin inhibition mediates sensitivity to chemotherapy and radiotherapy in human cancer. *Anticancer Drugs.* 2017;28(7):702–716.
  42. Yang CR, et al. Nuclear clusterin/XIP8, an x-ray-induced Ku70-binding protein that signals cell death. *Proc Natl Acad Sci U S A.* 2000;97(11):5907–5912.
  43. Uhlen M, et al. Towards a knowledge-based Human Protein Atlas. *Nat Biotechnol.* 2010;28(12):1248–1250.
  44. Marie-Egyptienne DT, et al. Cancer stem cells, the epithelial to mesenchymal transition (EMT) and radioresistance: potential role of hypoxia. *Cancer Lett.* 2013;341(1):63–72.
  45. Lee SY, et al. Induction of metastasis, cancer stem cell phenotype, and oncogenic metabolism in cancer cells by ionizing radiation. *Mol Cancer.* 2017;16(1):10.
  46. Aroeira LS, et al. Epithelial to mesenchymal transition and peritoneal membrane failure in peritoneal dialysis patients: pathologic significance and potential therapeutic interventions. *J Am Soc Nephrol.* 2007;18(7):2004–2013.
  47. Cannito S, et al. Epithelial-mesenchymal transition: from molecular mechanisms, redox regulation to implications in human health and disease. *Antioxid Redox Signal.* 2010;12(12):1383–1430.
  48. Zhou YC, et al. Ionizing radiation promotes migration and invasion of cancer cells through transforming growth factor-beta-mediated epithelial-mesenchymal transition. *Int J Radiat Oncol Biol Phys.* 2011;81(5):1530–1537.
  49. Gomez-Casal R, et al. Non-small cell lung cancer cells survived ionizing radiation treatment display cancer stem cell and epithelial-mesenchymal transition phenotypes. *Mol Cancer.* 2013;12(1):94.
  50. Sharma SV, et al. A chromatin-mediated reversible drug-tolerant state in cancer cell subpopulations. *Cell.* 2010;141(1):69–80.
  51. Dallas NA, et al. Chemoresistant colorectal cancer cells, the cancer stem cell phenotype, and increased sensitivity to insulin-like growth factor-I receptor inhibition. *Cancer Res.* 2009;69(5):1951–1957.
  52. Yin S, et al. Targeting the insulin-like growth factor-1 receptor by picropodophyllin as a treatment option for glioblastoma. *Neuro Oncol.* 2010;12(1):19–27.
  53. Fischer U, Meese E. Glioblastoma multiforme: the role of DSB repair between genotype and phenotype. *Oncogene.* 2007;26(56):7809–7815.
  54. McGranahan N, Swanton C. Clonal heterogeneity and tumor evolution: past, present, and the future. *Cell.* 2017;168(4):613–628.
  55. Bao S, et al. Glioma stem cells promote radioresistance by preferential activation of the DNA damage response. *Nature.* 2006;444(7120):756–760.
  56. Mannino M, Chalmers AJ. Radioresistance of glioma stem cells: intrinsic characteristic or property of the ‘microenvironment-stem cell unit’? *Mol Oncol.* 2011;5(4):374–386.
  57. Sampetean O, et al. Invasion precedes tumor mass formation in a malignant brain tumor model of genetically modified neural stem cells. *Neoplasia.* 2011;13(9):784–791.
  58. Alimpteri S, Andreadis ST. CDH2 and CDH11 act as regulators of stem cell fate decisions. *Stem Cell Res.* 2015;14(3):270–282.
  59. Groen RWJ, et al. N-cadherin-mediated interaction with multiple myeloma cells inhibits osteoblast differentiation. *Haematologica.* 2011;96(11):1653–1661.
  60. Ouyang M, et al. N-cadherin regulates spatially polarized signals through distinct p120ctn and  $\beta$ -catenin-dependent signalling pathways. *Nat Commun.* 2013;4:1589.
  61. Hellawell GO, et al. Expression of the type 1 insulin-like growth factor receptor is up-regulated in primary prostate cancer and commonly persists in metastatic disease. *Cancer Res.* 2002;62(10):2942–2950.
  62. Ma Y, et al. InsR/IGF1R pathway mediates resistance to egfr inhibitors in glioblastoma. *Clin Cancer Res.* 2016;22(7):1767–1776.
  63. Clemmons DR. Modifying IGF1 activity: an approach to treat endocrine disorders, atherosclerosis and cancer. *Nat Rev Drug Discov.* 2007;6(10):821–833.
  64. Osuka S, Van Meir EG. Overcoming therapeutic resistance in glioblastoma: the way forward. *J Clin Invest.* 2017;127(2):415–426.
  65. Van Meir EG, et al. Exciting new advances in neuro-oncology: the avenue to a cure for malignant glioma. *CA Cancer J Clin.* 2010;60(3):166–193.
  66. Ishii N, et al. Cells with TP53 mutations in low grade astrocytic tumors evolve clonally to malignancy and are an unfavorable prognostic factor. *Oncogene.* 1999;18(43):5870–5878.
  67. Kaur B, et al. Brain angiogenesis inhibitor 1 is differentially expressed in normal brain and glioblastoma independently of p53 expression. *Am J Pathol.* 2003;162(1):19–27.
  68. Willey CD, et al. Patient-derived xenografts as a model system for radiation research. *Semin Radiat Oncol.* 2015;25(4):273–280.
  69. Eustace NJ, et al. A cell-penetrating MARCKS mimetic selectively triggers cytolytic death in glioblastoma. *Oncogene.* 2020;39(46):6961–6974.
  70. Shimizu T, et al. c-MYC overexpression with loss of Ink4a/Arf transforms bone marrow stromal cells into osteosarcoma accompanied by loss of adipogenesis. *Oncogene.* 2010;29(42):5687–5699.
  71. Fujino RS, et al. Spermatogonial cell-mediated activation of an IkappaBzeta-independent nuclear factor-kappaB pathway in Sertoli cells induces transcription of the lipocalin-2 gene. *Mol Endocrinol.* 2006;20(4):904–915.
  72. Walker K, Hjelmeland A. Method for efficient transduction of cancer stem cells. *J Cancer Stem Cell Res.* 2014;2:e1008.
  73. Zhu D, et al. BAI1 suppresses medulloblastoma formation by protecting p53 from Mdm2-mediated degradation. *Cancer Cell.* 2018;33(6):1004–1016.
  74. Harusato A, et al. IL-36 $\gamma$  signaling controls the induced regulatory T cell-Th9 cell balance via NF $\kappa$ B activation and STAT transcription factors. *Mucosal Immunol.* 2017;10(6):1455–1467.
  75. Shimizu T, et al. IGF2 preserves osteosarcoma cell survival by creating an autophagic state of dormancy that protects cells against chemotherapeutic stress. *Cancer Res.* 2014;74(22):6531–6541.